Our progress towards linearized waveform inversion with velocity updating (LWIVU)

Alejandro Cabrales-Vargas, Biondo Biondi, and Robert Clapp

ABSTRACT

Linearized waveform inversion with velocity updating demands the cooperation of Born modeling and wave-equation migration velocity analysis, both forward modeling operators and their adjoints. We successfully tested both of them for passing both the dot-product test and the linearization test. We previously re-organized the wave-propagation codes to operate with random boundary conditions, thus achieving more efficient RAM usage. Assuming the correctness of the operators after the tests, we use the Born modeling pair to illustrate how to pre-compute the Gauss-Newton Hessian by means of point-spread functions. We have now the elements to assemble a robust code for linearized waveform inversion with velocity updating.

INTRODUCTION

We introduced the concept of linearized waveform inversion with velocity updating (LWIVU) in the last SEP reports (Cabrales-Vargas et al., 2016a,b). This technique constitutes an attempt to improve the estimated reflectivity by accounting for remnant inaccuracies in the velocity model which, however too small to induce mispositioning of reflectors, can in turn produce inaccuracies in the estimated reflectivity. Whereas one may disregard such imprecisions as "trifles" for exploration purposes, well positioning in reservoir characterization can significantly rely upon careful and accurate handling of amplitude contrasts, which often reflect reservoir variations such as fluid content, sedimentary facies, dissolution and collapse features, etc. LWIVU can potentially minimize the occurrence of amplitude variations unrelated to reservoir rock properties. Hence, we envision its application mainly to small seismic volumes for detailed studies.

LWIVU is fundamentally based upon the fact that the full waveform inversion (FWI) Hessian (henceforth referred to as "full Hessian") can be split into the sum of the Gauss-Newton Hessian (henceforth referred to simply as "Hessian") and the wave-equation migration velocity analysis (WEMVA) operator (Biondi et al., 2015). These operators are applied to the search direction in the model parameters in the Newton's equation. Regarding the search direction as a *perturbation in the model parameters* we in turn split it into a perturbation in the background model (slowness squared) and a perturbation in the reflectivity. The other side of the Newton's equation, the negative

of the gradient of the FWI misfit function, becomes the conventional reverse-time migration (RTM) of the field data. We refer the reader to the aforementioned reports for details. We have very succinctly summarized the derivation here to emphasize that LWIVU demands the interactivity of two operators (with their adjoints) that need be carefully tested, lest numerical errors and/or even unphysical results affect the inversion.

We report the progress in preparing the "pieces of the puzzle", *e.g.*, the operators that conform LWIVU. The aspects discussed in this report are a) Incorporation of random boundary conditions in Born modeling (forward and adjoint) and in WEMVA; b) Linearization test, complementary to the classic dot-product test; c) Use of point-spread-functions (PSF) to compute elements of the Hessian. A significant step, not addressed in this report, is that we re-wrote the codes in modern Fortran, including object-oriented programming. This paradigm improves organization and readability, and potentially facilitates the future transition to C++.

IMPLEMENTATION

Random boundary conditions

Random boundary conditions (RBC) in RTM (Clapp, 2009; Shen and Clapp, 2011; Clapp and Alves, 2016) constitute an alternative to checkpointing (*e.g.*, Symes, 2007). They consist of a halo or extended region around the velocity model. We progressively introduce random variations of velocity when entering such region, increasing randomness as going further inside. At the same time we make the velocity trend ramp down. The overall effect is "scrambling" and delaying the unphysical reflection from the ultimate computational frontier. In RTM we employ RBC in the source wavefield propagation, driving boundary reflections to becoming randomly incoherent from source to source. Stacking the migrated shots reinforces the signal and weakens the random and incoherent reflections from the boundary.

This procedure aims at making the source wavefield propagation reversible in time, unlike propagation using damping boundary conditions (DBC) (Cerjan et al., 1985). Figure 1 illustrates the comparison between RTM performed using DBC (top) and RBC (bottom). DBC require the storage of at least one wavefield (a), usually the source wavefield (orange boxes), as the receiver wavefield (blue boxes) is propagated backward (b-g). Cross-correlations are performed to construct the image (red rectangles). As wavefields may consist of hundreds or thousands of time frames, limitations in RAM or disk storage, particularly in 3-D, are obvious. On the contrary, with RBC we save two time frames of the source wavefield at the final time (a), then propagate it backward jointly with the receiver wavefield and performing the cross-correlations at each time step. Only four time frames are kept in memory during the process. The memory saving using RBC come at the price of an additional propagation of the source wavefield.

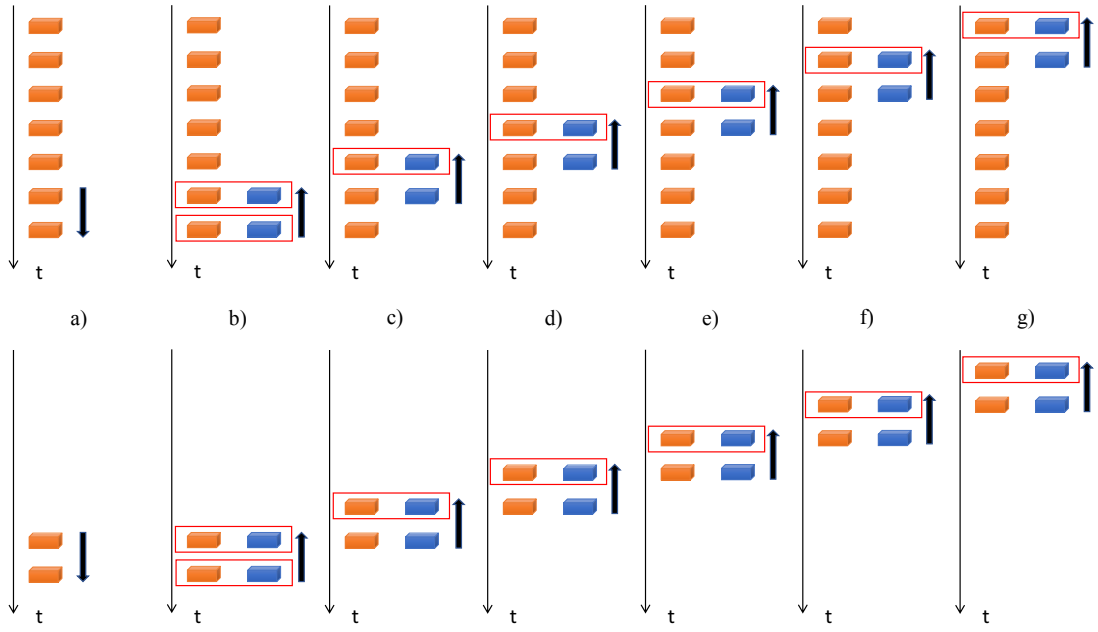

Figure 1: .
]Schematic showing the comparison between RTM implementations using *top*: conventional damping boundary conditions; *bottom*: random boundary conditions. Orange boxes represent source wavefield time frames and blue boxes represent receiver wavefield time frames. See text for explanation. [**NR**].

We too incorporate RBC in WEMVA. Using DBC, WEMVA requires four propagations: 1) source wavefield; 2) receiver wavefield; 3) source scattered wavefield; and 4) receiver scattered wavefield. With RBC we need an extra propagation of the source wavefield. Figure 2 shows a pseudocode of this procedure in three stages. Note that we use RBC when wavefields need be reversed. We *must not* use DBC in such cases. The scattered wavefields are not reversed, therefore they can be damped at the boundaries. The same situation occurs with the source wavefield during the third stage. Note the order of the injections of source/data and the scaling factors. We follow the scheme analyzed by Almomin (2013) in our RTM and WEMVA implementations, in order to ensure the correct linearization of the operators.

Linearization tests

For many years the SEP crew has been using (almost religiously) the dot-product test in code debugging (Claerbout, 2014) for inversion purposes. The formula is simple: If your code fails the test, this means that your linear forward/adjoint operators are not really adjoint of each other, and you ought to debug. However, if your code passes the test, you might have coded operators which, notwithstanding their mutual adjointness, may not be representative of the physical phenomenon that you intend to linearize. In order to prevent this scenario we perform the linearization test.

The linearization test consists on verifying that our linearized operator, $\mathbf{F}$, resembles the action of the full nonlinear operator, $\mathcal{F}$, in the presence of small perturbations in the model parameters, $\mathbf{\Delta m} = \mathbf{m} - \mathbf{m}_0$:

$$\mathcal{F}(\mathbf{m}) - \mathcal{F}(\mathbf{m}_0) \approx \mathbf{F}\mathbf{\Delta m}, \tag{1}$$

where $\mathbf{m}$ and $\mathbf{m}_0$ are the perturbed model and the background model, respectively.

In preparation for the LWIVU implementation we performed the linearization test on Born modeling and WEMVA after passing the dot-product test. In Born modeling, the perturbed model parameter is slowness squared, $\mathbf{s}^2 = \mathbf{s}_0^2 + \mathbf{\Delta s}^2$, which induces a perturbation in the data, $\mathbf{\Delta d} = \mathcal{L}(\mathbf{s}^2) - \mathcal{L}(\mathbf{s}_0^2) \approx \mathbf{L}\mathbf{\Delta s}^2$, where $\mathcal{L}$ represents the nonlinear acoustic wave-equation modeling operator, and $\mathbf{L}$ represents the Born modeling operator. In WEMVA modeling, the perturbed model parameter is slowness squared too, this time inducing a perturbation in the migration image, $\mathbf{\Delta I} = \mathbf{I}(\mathbf{s}^2) - \mathbf{I}(\mathbf{s}_0^2) \approx \mathbf{W}\mathbf{\Delta s}^2$, where $\mathbf{I}(\mathbf{s}^2)$ and $\mathbf{I}(\mathbf{s}_0^2)$ are the migration images corresponding to the perturbed and the background slownesses squared respectively, and $\mathbf{W}$ represents the WEMVA operator.

Figure 3 shows the results of the linearization test for our Born modeling operator. We pertubed a constant slowness squared model with a single impulse that represents a 3% increment of amplitude in the corresponding background velocity model. The corresponding perturbation in the data is a single diffraction. The comparison between the exact result (left panel) and the approximated (linearized) result (right panel) demonstrates that our Born modeling operator effectively represents the

```
1st stage: Forward propagation of source wavefield
do in time steps (forward)
   Propagate the source wavefield one time step;
   Scale the source function;
   Inject the source function;
end do

2nd stage: Backward propagation of receiver wavefield+scattering
and cross-correlation with backward propagated source wavefield
do in time steps (backward)
   Inject the data;
   Propagate receiver wavefield and source wavefield one time step;
   Scale source function;
   Re-inject the source function;
   Scale the receiver wavefield;
   Scatter the receiver wavefield;
   Propagate scattered receiver wavefield;
   Damp scattered receiver wavefield at the boundaries;
   WEMVA_receiver_side += xcorr(source wavefield, scattered receiver wavefield)
end do

3rd stage: Forward propagation of source wavefield+scattering
and cross-correlation with forward propagated receiver wavefield
do in time steps (forward)
   Re-inject the data;
   Propagate source wavefield and receiver wavefield one time step;
   Scale the receiver wavefield;
   Scale source function;
   Inject the source function;
   Damp source wavefield at the boundaries;
   Scale the source wavefield;
   Scatter the source wavefield;
   Propagate the scattered source wavefield;
   Damp scattered source wavefield at the boundaries;
   WEMVA_source_side += xcorr(receiver wavefield, scattered source wavefield)
end do
```

Figure 2: .
]Pseudocode for the implementation of WEMVA using RBC [**NR**].

linearization of the full wave-equation modeling operator. The panels share the same scaling and are not clipped.

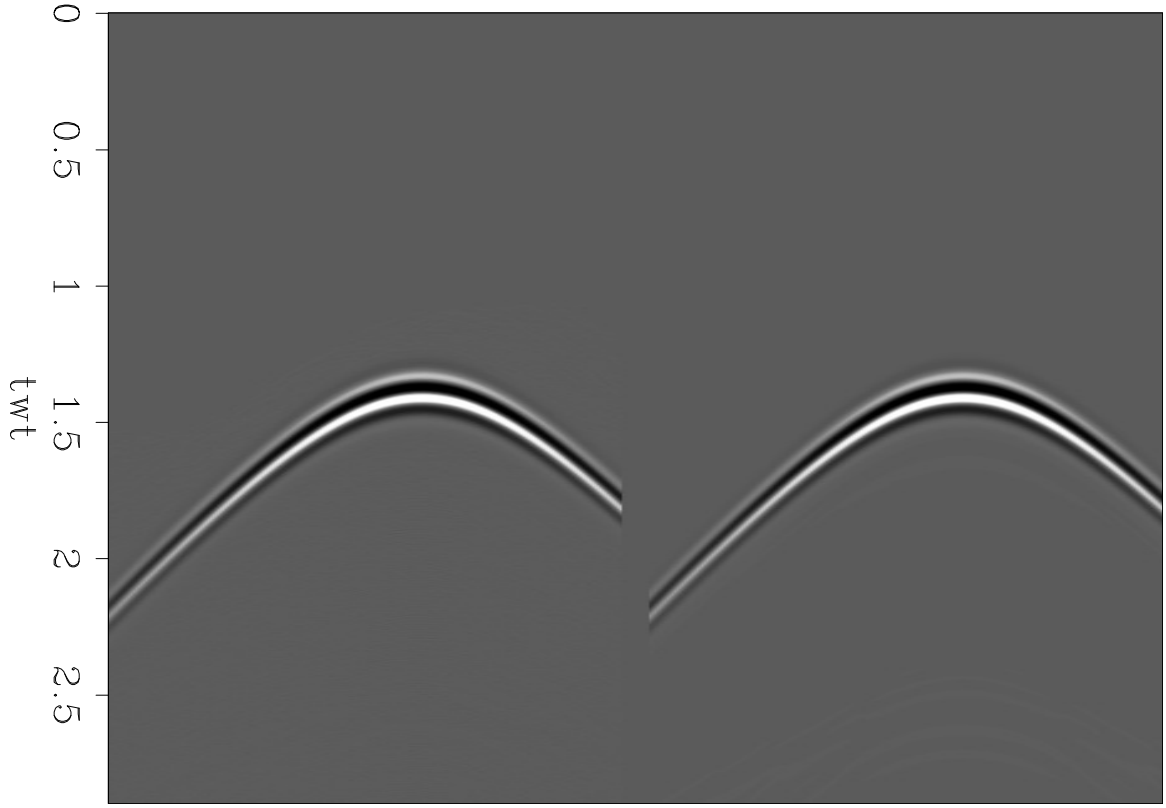

Figure 3: .
]Linearization test of the Born operator. *Left panel*: Perturbation in the data obtained with the full nonlinear wave equation operator. *Right panel*: Perturbation in the data approximated with the Born modeling operator [**ER**].

Similarly, Figure 4 shows the results of the linearization test for our WEMVA operator. The perturbation in the image is produced by the same perturbation in slowness squared as in the previous test. The dataset employed in this experiment is a single shot gather of the Marmousi model. Note the "banana-doughnut" kernel with foci at the source and the slowness squared perturbation positions. Except for some artifacts at the surface in the WEMVA panel (right), the exact result (left panel) and the approximated result (right panel) of the perturbation in the image are virtually equivalent.

Precomputing the Gauss-Newton Hessian using point spread functions

We use the Born forward/adjoint linear operators to pre-compute the Hessian using the concept of PSFs (Fletcher et al., 2016). We first "seed" unit spikes uniformily

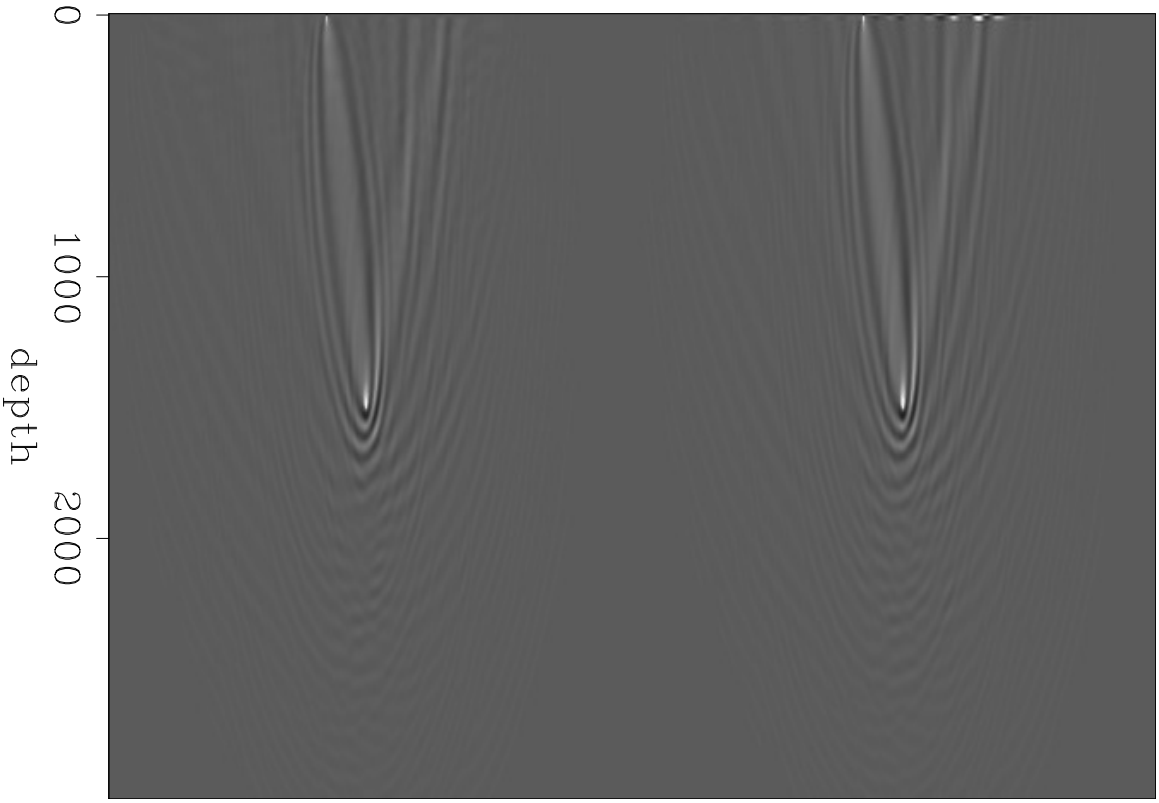

Figure 4: .
]Linearization test of the WEMVA operator. *Left panel*: Perturbation in the image obtained with the RTM operator. *Right panel*: Perturbation in the image approximated with the WEMVA operator [**ER**].

scattered over the image space. Applying forward Born modeling followed by the adjoint (RTM) we obtain "blurred" or smeared spikes (Hu et al., 2001) that conform the PSFs. They constitute the impulse response of the Hessian at the spike locations. Figure 5 shows PSFs obtained in the Marmousi model after seeding spikes every 30 points both in depth and distance. The diagonal of the Hessian matrix corresponds to amplitude values picked at the center of the PSFs, *e.g.*, the values at the position of the original input spikes. Likewise, off-diagonal elements of the Hessian are picked at determined lags with respect to diagonal elements. We interpolate afterwards to get Hessian elements all over the model space. Figure 6 shows the diagonal of the Hessian after 2-D linear interpolation. Note that this kind of interpolation exhibits poor performance mainly due to the large separation of the points. Increasing the density of the spikes yields to interference that induce imprecision in the amplitudes of the PSFs. We can use a more robust interpolation scheme or more than one spike assemblage, where spikes are sparse and cover different positions in each assemblage (Fletcher et al., 2016). As we write this report we evaluate both approaches.

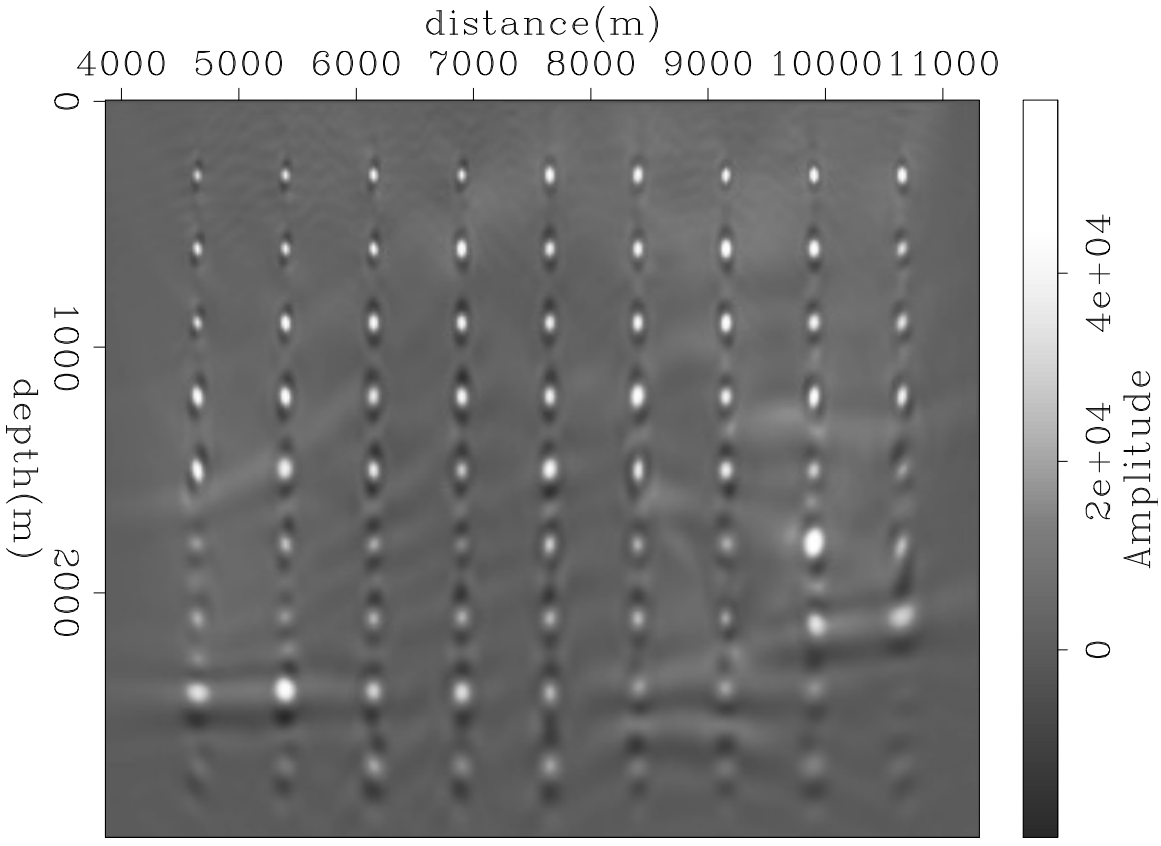

Figure 5: .
]Point-spread functions computed in the Marmousi model. [**ER**].

In Figure 7 we show LWI performed in model space, employing exclusively the diagonal of the Hessian (Figure 6). For comparison, Figure 8 shows the result of LWI in data space. Both inversions were run for 10 iterations. As expected, the former constitutes a scaled version of the RTM image, with some noise introduced by the

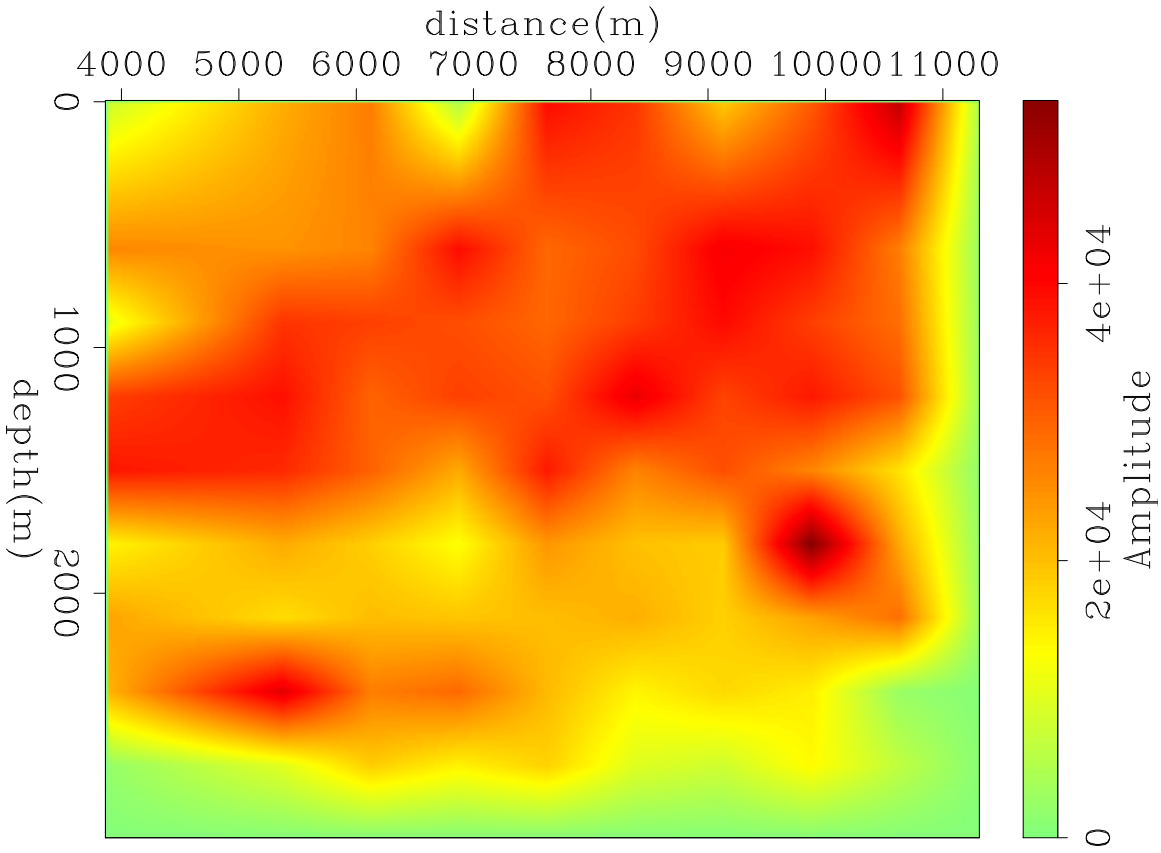

Figure 6: .
]Diagonal of the Hessian approximated from the interpolation of scattered points picked from the PSF (Figure 5). [**ER**].

imperfect interpolation. Nonetheless, it leads the amplitude to the correct values (compare the scale bars), encouraging us to definitely adopt this technique in our Hessian computation.

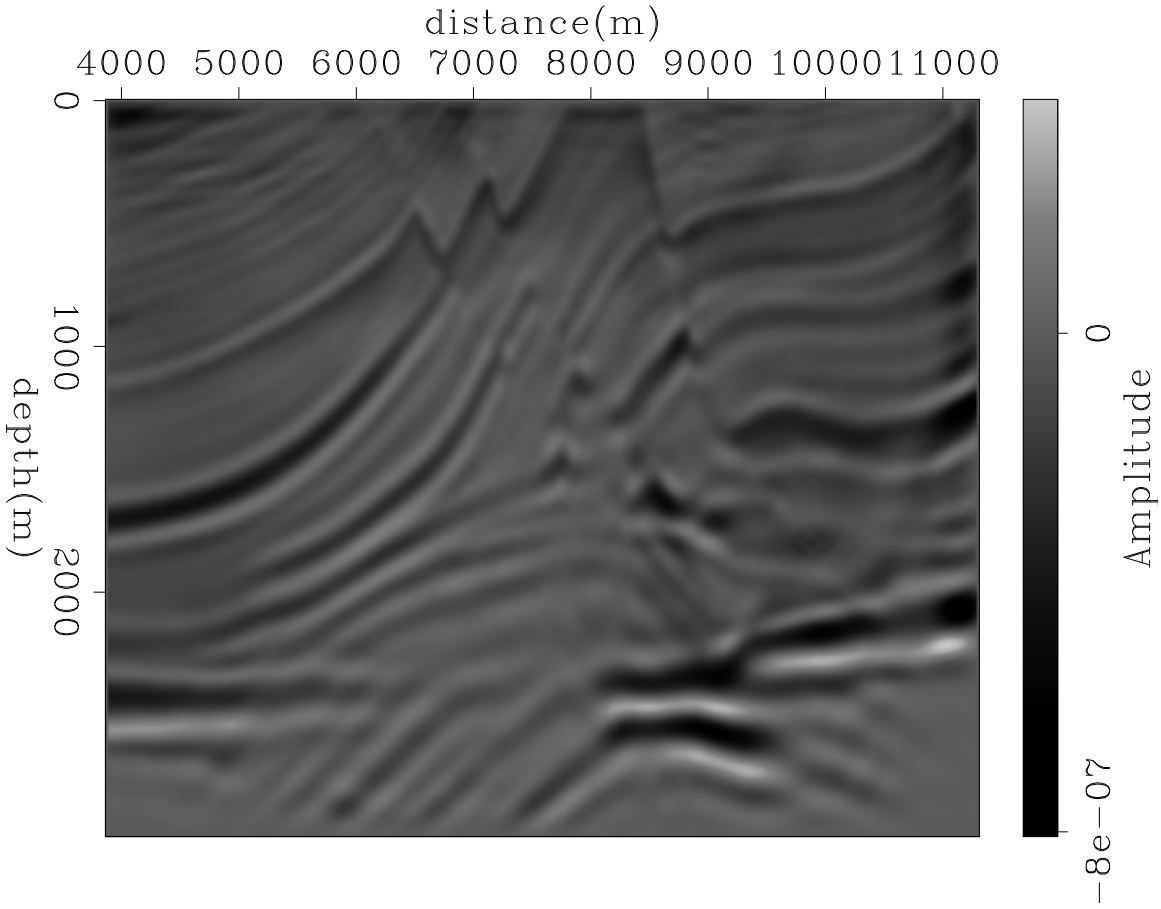

Figure 7: .
]LWI of the Marmousi model in model space, using the diagonal of the Hessian. [**ER**].

FUTURE WORK

In Cabrales-Vargas et al. (2016a,b) we expressed the full Hessian as the sum of the Gauss-Newton Hessian, $\mathbf{H}_{GN}$, and WEMVA, $\mathbf{H}_W$, (Biondi et al., 2015) and expanded the perturbation of the model parameters, $\mathbf{\Delta m}$, into a perturbation in the background model, $\mathbf{\Delta b}$, and a perturbation in the reflectivity, $\mathbf{\Delta r}$:

$$\mathbf{H\Delta m} = (\mathbf{H}_{GN}+\mathbf{H}_W)(\mathbf{\Delta r}+\mathbf{\Delta b}) = (\mathbf{H}_{GN}\mathbf{\Delta r}+\mathbf{H}_W\mathbf{\Delta b})+(\mathbf{H}_W\mathbf{\Delta r}+\mathbf{H}_{GN}\mathbf{\Delta b}). \quad (2)$$

We kept the first part of the right-hand side of Equation 2, whereas neglected the second part as it contains terms that we do not wish to include in the inversion.

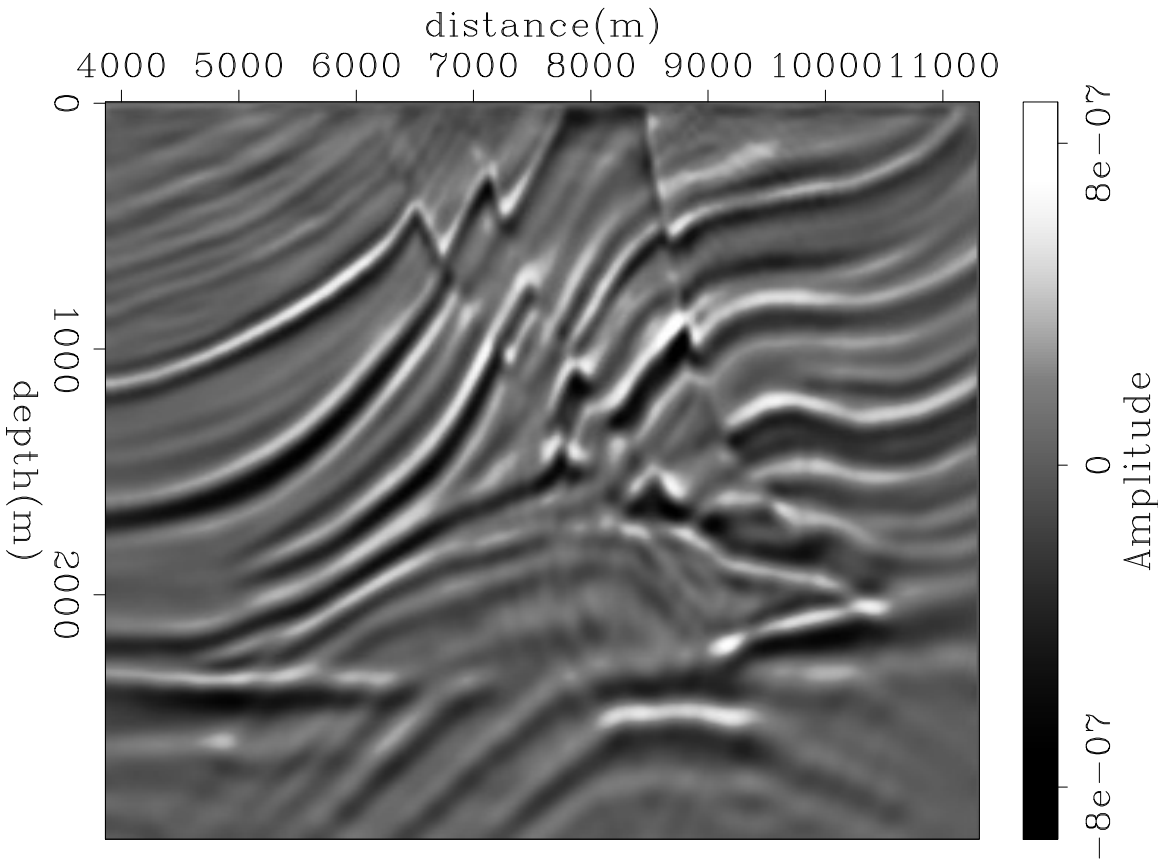

Figure 8: .
]LWI of the Marmousi model in data space. [**CR**].

We will design and performing numerical experiments aimed at analyzing each term's response, for the sake of understanding the significance of their absence from LWIVU.

The next step is the inclusion of off-diagonal elements of the Hessian in the inversion, followed by the construction of LWIVU with the operators shown in this report.

CONCLUSIONS

In this report we showed the progress in the construction of reliable Born modeling and wave-equation migration velocity analysis operators, intended to work together in the linearized waveform inversion with velocity updating process. The incorporation of random boundary conditions hugely reduced the computational storage burden, enabling us to perform future tests with large datasets. With the classical dot-product test and the recently adopted linearization test, we ensure both the "adjointness" of the operators and their correctness in portraying linearization at the presence of small perturbations in the model parameters. Finally, we showed the application of Born forward/adjoint pair in the computation of point-spread functions for fast and practical computation of the Gauss-Newton Hessian.

ACKNOWLEDGEMENTS

We would like to thank the SEP sponsors for their continuous support. Alejandro Cabrales would like to thank Petróleos Mexicanos for financing his studies in Stanford. Special thanks to Ettore Biondi for his assistance and advices with regards of the linearization test.

REFERENCES

Almomin, A., 2013, Accurate implementation of two-way wave-equation operators: SEP-Report, **149**, 281–288.

Biondi, B., E. Biondi, M. Maharramov, and Y. Ma, 2015, Dissection of the full-waveform inversion hessian: SEP-Report, **160**, 19–38.

Cabrales-Vargas, A., B. Biondi, and R. Clapp, 2016a, Linearized waveform inversion with (small) velocity updating : SEP-Report, **163**, 189–196.

———, 2016b, Linearized Waveform Inversion with Velocity Updating: Theory and first results : SEP-Report, **165**, 63–92.

Cerjan, C., D. Kosloff, R. Kosloff, and M. Reshef, 1985, A nonreflecting boundary condition for discrete acoustic and elastic wave equations: Geophysics, **50**, 705–708.

Claerbout, J. F., 2014, Geophysical image estimation by example: Jon Claerbout.

Clapp, R., 2009, Reverse time migration with random boundaries: SEG Technical Program Expanded Abstracts, 2809–2813.

Clapp, R. G. and G. Alves, 2016, Random boundaries for elastic medium : SEP-Report, **163**, 41–48.

Fletcher, R., D. Nichols, R. Bloor, and R. Coates, 2016, Least-squares migation - data domain versus image domain using point spread functions: The Leading Edge, **35**, no. 2, 157–162.

Hu, J., G. Schuster, and P. Valasek, 2001, Poststack migration deconvolution: Geophysics, **66**, 939–952.

Shen, X. and R. Clapp, 2011, Random boundary condition for low-frequency wave propagation: SEG Technical Program Expanded Abstracts, 2962–2965.

Symes, W., 2007, Reverse time migration with optimal checkpointing: Geophysics, **72**, no. 5, SM213–SM221.